NSG-1316

ELECTRON PARAMAGNETIC RESONANCE STUDIES OF SLOWLY TUMBLING VANADYL SPIN PROBES IN NEMATIC LIQUID CRYSTALS

by

G. V. Bruno, J. K. Harrington, and M. P. Eastman

Department of Chemistry
University of Texas at El Paso
El Paso, Texas 79968

(NASA-CR-157609) ELECTRON PARAMAGNETIC RESONANCE STUDIES OF SLOWLY TUMBLING VANADYL SPIN PROBES IN NEMATIC LIQUID CRYSTALS (Texas Univ. at El Paso.) 35 p HC A03/MF A01 CSCL 20B G3/76

N78-32895

Unclas
30288

Abstract:

An analysis of EPR line shapes by the method of Polnaszek, Bruno, and Freed is made for slowly tumbling vanadyl spin probes in viscous nematic liquid crystals. The use of typical vanadyl complexes as spin probes for nematic liquid crystals is shown to simplify the theoretical analysis and the subsequent interpretation. Rotational correlation times τ and orientational ordering parameters S_z where slow tumbling effects are expected to be observed in vanadyl EPR spectra are indicated in a plot. Spectral EPR line shapes were simulated for experimental spectra of vanadyl acetylacetonate (VOAA) in nematic butyl-p-(p-ethoxyphenoxycarbonyl) phenyl carbonate (BEPC) and Phase V of EM Laboratories. Two factors are important in achieving good agreement with experimental spectra. The primary factor results from the slow tumbling undergone by VOAA in these viscous solvents. A secondary factor arises from the non-Brownian rotation of the small VOAA probe. Analysis of the inertial effects on the probe reorientation, which are induced by slowly flucuating torque components of the local solvent structure, yield quantitative values for τ and S_z. Similar effects were previously reported by Polnaszek and Freed for the small perdeuterated 2,2,6,6-tetramethyl-4-piperidone N-oxide (PD-tempone) nitroxide spin probe. The weakly ordered probe VOAA is in the slow tumbling region and displays these inertial effects throughout the nematic range of BEPC and Phase V. VOAA exhibits different reorientation behavior near the isotropic-nematic transition temperature (within $\sim 15^{0}$C) than that displayed far below this transition temperature.

Introduction

The application of paramagnetic spin probes in a variety of experiments has resulted in obtaining a wide range of structural and dynamical information.[1,2] Of particular interest to us is the use of complexes containing the vanadyl ion VO^{2+} as spin probes.[3-6] In a recent paper, we had applied the stochastic Liouville method to calculate EPR line shapes in the slow tumbling region for vanadyl complexes in an isotropic medium.[7] This analysis allows one to extract quantitative information from the EPR line shapes for rotational correlation times τ in the range $\sim 10^{-10} - 10^{-7}$ sec/rad. These slow tumbling EPR spectra occur when the vanadyl ion is rigidly attached to a macromolecule[5] or when a vanadyl complex is dissolved in a viscous solvent.[8,9]

We now want to extend our analysis of slowly tumbling vanadyl spin probes in an isotropic medium to that in an anisotropic medium. An example of current interest is the study by EPR of nematic liquid crystals doped with paramagnetic probes.[4,10] Appropriate analysis of the EPR spectra yields information of molecular orientational ordering and molecular reorientational dynamics.[4,11-13] Because liquid crystals, especially the electro-optically important room temperature nematogens,[14] are highly viscous by nature, slow tumbling EPR spectra have been obtained for both nitroxide[10] and vanadyl[8,9] spin probes. Since the slow tumbling region for vanadyl complexes occurs at a shorter τ than for nitroxide spin probes, vanadyl complexes of comparable size to the nitroxide spin probe should more readily exhibit EPR spectra with slow tumbling features.

A primary reason that vanadyl complexes are excellent probes for nematic liquid crystals is that they have nearly axially symmetric magnetic parameters

which is the same degree of symmetry possessed by the nematic liquid crystals.[4,15] The subsequent theoretical analysis is simplified and the results are easier to interpret than for typical nitroxide spin probes with less symmetry.[10] Also, the characteristic eight hyperfine line EPR spectrum of vanadyl complexes provides a more severe testing of any theoretical analysis than a three hyperfine line nitroxide spectrum would provide. In addition, inhomogeneous broadening is usually neglible in the EPR spectra of vanadyl complexes. Previous workers recognized these features of vanadyl spin probes but have encountered difficulty in the quantitative interpretation of the EPR spectra because of slow tumbling aspects.[8,9]

There are three main objectives for this paper. One is to establish when the breakdown of motionally narrowed formulae occurs.[12,16] A second objective is to analyze the experimental vanadyl EPR line shapes by the stochastic Liouville method[17] as developed by Polnaszek, Bruno, and Freed (PBF)[13] for slow tumbling in an anisotropic liquid. Third is comparison of our vanadyl probe study to the detailed work of Polnaszek and Freed[10] who reported anamolous behavior for the perdeuterated 2,2,6,6-tetramethyl-4-piperidone N-oxide (PD-tempone) nitroxide spin probe.

Vanadyl acetylacetonate (VOAA) was used as the vanadyl spin probe because it has excellent EPR spectroscopic and physical properties and because it has essentially axially symmetric magnetic parameters.[18] An additional advantage arises from our previous detailed work with VOAA in a viscous isotropic medium.[7] The nematic mixture Phase V from EM Laboratories was studied because it is a nematic at low temperatures and has a wide nematic temperature range. A second low temperature nematic liquid crystal, butyl-p-(p-ethoxyphenoxycarbonyl) phenyl carbonate (BEPC), which is a single

component liquid crystal, was also studied for comparison.

Experimental

Degassed samples of nematic liquid crystals doped with VOAA were prepared by standard vacuum line techniques. VOAA was purchased from Alfa Products and was purified by recrystallization from acetone.[19] The nematic liquid crystal BEPC was obtained from Eastman Chemicals and was recrystallized from methanol and then from benzene.[10] The nematic mixture Phase V was purchased from EM Laboratories and used without further purification.

EPR spectra were taken on a Varian V-4500 spectrometer with 100 kHz modulation. Varian E-257 variable temperature unit controlled the temperature to ±1 K over the active region of the cavity. The magnetic field was measured with a Brucker BNM-12 tracking magnetometer, which was used for spectral calibration. The microwave frequency was obtained with a Hewlett Packard 5248 L electronic counter and 5257A transfer oscillator.

Theory

A. Slow Tumbling

PBF[13] have developed a general method for calculating slow tumbling EPR line shapes in an anisotropic liquid. This approach is based upon the stochastic Liouville method[17,20] and is a generalization of an analysis by Nordio and co-workers for the motionally narrowed EPR line widths of a Brownian particle in a liquid crystal.[12] Here, we apply the general PBF approach to vanadyl spin probes in viscous nematic liquid crystals.

Previous detailed studies in an isotropic solvent have shown that the spin Hamiltonian for VOAA has very nearly axially symmetric magnetic interactions.[18,7] The motionally narrowed line widths ($\tau < 8 \times 10^{-11}$ sec/rad)

calculated with axially symmetric parameters differ by less than 0.5% from those calculated with completely asymmetric tensor values.[18] Our slow tumbling study of VOAA in toluene showed that the use of axially symmetric parameters gave very good agreement with experimental line shapes for the slow tumbling range of $\tau \sim 8 \times 10^{-11} - 1 \times 10^{-9}$ sec/rad.[7] Only for EPR line shapes ($\tau > 1 \times 10^{-8}$ sec/rad) very close to the rigid limit spectrum would the use of completely asymmetric parameters improve the fit to experimental spectra.[21]

The orientational portion of the pseudo-potential $u(\theta)$ for nematic liquid crystals may be expressed by an expansion

$$u(\theta) = \sum_{n \text{ even}}^{\infty} \gamma_n \cos^n\theta \qquad (1)$$

where θ is the angle between the molecular long axis and the director.[22] Because VOAA has the same degree of symmetry as the nematic liquid crystalline solvent, the form of Eq. (1) should also reflect the orientational restoring potential for VOAA. In our experiments, the small VOAA is moderately ordered. Previous studies have shown that EPR spectral line shapes are not sensitive to γ_4 variations.[13] Thus a simple Maier-Saupe potential[23]

$$u'(\theta) \simeq \gamma_2' \cos^2\theta \qquad (2)$$

is suitable to describe VOAA. (The prime refers to the spin probe values.) In Eq. (2), θ is the angle between the VO bond (molecular z axis) and the director. Note that VOAA, an oblate symmetric top molecule, has $\theta_{eq} = \frac{\pi}{2}$ so that γ_2' is positive. Eq. (2) leads to a Boltzmann equilibrium $P_o(\theta)$

given by[12]

$$P_o(\theta) = \exp(\lambda \cos^2\theta) / \int_o^{\pi} d\theta \sin\theta \exp(\lambda \cos^2\theta) \tag{3}$$

where

$$\lambda = -\gamma_2'/kT \ . \quad \lambda < 0 \text{ for VOAA.} \tag{4}$$

An orientational ordering parameter S_z is then defined[23] by

$$S_z = \langle P_2(\theta) \rangle \tag{5}$$

$$= \int_o^{\pi} d\theta \sin\theta \, P_2(\theta) \, P_o(\theta) \tag{6}$$

where

$$P_2(\theta) = \frac{1}{2}(3\cos^2\theta - 1) \tag{7}$$

For complete alignment where $P_o(\theta) = \delta(\theta - \frac{\pi}{2})$, $S_z = -\frac{1}{2}$.

For a Brownian particle under a restoring potential Eq. (2), matrix elements of the symmetric rotational diffusion operator $\tilde{\Gamma}$ are given by[13]

$$\frac{N(L,L')}{8\pi^2} \left\langle D^L_{Om} \middle| \tilde{\Gamma} \middle| D^{L'}_{Om'} \right\rangle = [R_\perp L(L+1) + (R_{11} - R_\perp)m^2 + \frac{2}{15} R_\perp \lambda^2] \delta_{LL'} \, \delta_{mm'}$$

$$- 2R_\perp \lambda (1 - \frac{\lambda}{21})(-1)^m N(L,L') \begin{pmatrix} L & 2 & L' \\ 0 & 0 & 0 \end{pmatrix} \begin{pmatrix} L & 2 & L' \\ -m & 0 & m \end{pmatrix} \delta_{mm'}$$

$$- \frac{8}{35} R_\perp \lambda^2 (-1)^m N(L,L') \begin{pmatrix} L & 4 & L' \\ 0 & 0 & 0 \end{pmatrix} \begin{pmatrix} L & 4 & L' \\ -m & 0 & m \end{pmatrix} \delta_{mm'} \tag{8}$$

Eq. (8) is appropriate for anisotropic viscosity where $R_\perp$ and R_{11} are rotational diffusion constants perpendicular and parallel, respectively, to the director. Normalization factor $N(L,L')$ is $[(2L+1)(2L'+1)]^{1/2}$, D^L_{om} are

Wigner rotation matrices, and $\begin{pmatrix} L & n & L' \\ -m & 0 & m \end{pmatrix}$ are 3-j symbols.[24] Note that effects of anisotropic viscosity are proportional to $(R_{11} - R_{\perp})m^2$.

The application of the general methods in PBF to the VOAA spin probe indicate its simplified nature. In addition to the simple one-term potential Eq. (2), VOAA has the principal axes of its magnetic parameters (g and A tensors) coinciding with the molecular rotational coordinate frame. One need not incorporate tilt angles and additional transformations of coordinate symstems into the orientation-dependent portion of the spin Hamiltonian (other than usual one that is done even for isotropic solvents).

Appendix A explicitly presents a convenient set of equations whose solution yields the unsaturated EPR line shapes for vanadyl spin probes undergoing Brownian rotation (Eq.8) in nematic liquid crystal. Nonsecular contributions, in addition to those given for the isotropic solvent,[7] are also included. In these equations, the director is parallel to the external magnetic field. This alignment is the usual case in nematic liquid crystals.[25]

A second method of solution allows for modifications that arise from non-Brownian diffusion. This method involves the numerical diagonalization of Eq. [8] (a real symmetric matrix) to obtain eigenvalues E^n_{om} and eigenfunctions u^n_{om}.

$$u^n_{om} = \sum_L a^{(n)L}_{om} D^L_{om} \tag{9a}$$

$$E^n_{om} = \langle u^n_{om} | \tilde{\Gamma} | u^n_{om} \rangle \tag{9b}$$

where the coefficients $a^{(n)L}_{om}$ form column vectors of the post-matrix in the diagonalization transformation. In general, eight diagonalizations

would be performed for vanadyl (corresponding to the eight m values). Deviations from Brownian rotation may be expected for the small VOAA probe dissolved in the much larger liquid crystal solvent molecules. One worthwhile modification is an analysis of inertial effects[26] to lowest order, which are induced on VOAA by slowly flucuating torque components from the local solvent structure.[27,28] Polnaszek and Freed[10] applied this analysis to nitroxide spin probes embedded in a liquid crystal solvent. Polnaszek[29] gives details for obtaining equations for the slow tumbling region. Specific equations are given in Appendix B. An essential point of this approach is that factors $\epsilon'_{L,m}$ (> 1) are introduced to indicate deviations from Brownian rotation. Values $\epsilon'_{L,m} = 1$ yield Brownian rotation diffusion. In a motionally narrowed analysis, $\epsilon'_{2,m}$ would correspond to correction factors in the spectral density functions. For $R_\perp = R_{11} = \frac{1}{6\tau}$ and low ordering, $\epsilon'_{2,0}$ (ϵ'_{sec}) and $\epsilon'_{2,m\neq 0}$ (ϵ'_{psec}) reflect the relative effective torque components (i.e., parallel and perpendicular, respectively, to the director) which affect reorientation of the probe.

B. Motionally Narrowed Region

PBF[13] describe a convenient method for obtaining line widths from the real part of the spectral density function $K(m,\omega)$ given by

$$\text{Re } K(m,\omega) = \sum_{n\neq 0} \frac{(-1)^m E_n}{E_n^2 + \omega^2} \langle u_o | D^2_{om} | u_n \rangle \langle u_n | D^2_{o,-m} | u_o \rangle \qquad (10)$$

where E_n and u_n are the eigenvalues and eigenfunctions of Eq. (9). Those nonsecular terms which arise from the large intramolecular magnetic interactions are treated firstly by a perturbation analysis.[7,13] Linewidth contributions from these terms are then obtained by the method in PBF.[13] Such an analysis yields a cubic dependency (δm^3) in the line width expression.[4,7,18] The first derivative line width (in gauss), which is similar to the one given for isotropic solvents,[7] may be written

$$\Delta H(m) = \alpha + \beta m + \gamma m^2 + \delta m^3 \qquad (11)$$

where

$$\alpha = \alpha'' + \frac{2\,\mathrm{Re}}{\sqrt{3}\,|\gamma_e|}\left\{F^2\left[K(0,0) + \frac{3}{4}K(0,\omega_o) + \frac{3}{14}\frac{F}{\omega}K(0,0)\right]\right.$$

$$+ I(I+1)D^2\left[K(1,\omega_a) + 2K(2,\omega_o) + \frac{1}{3}K(0,\omega_o)\right.$$

$$+ \frac{5F}{7\omega}\left(K(1,\omega_a) - \frac{4}{3}K(0,0)\right)$$

$$\left.\left. + \sqrt{\frac{8}{3}}\,\frac{FDa}{\omega}\left(K(0,0) - \frac{3}{4}K(1,\omega_a)\right)\right]\right\} \qquad (12a)$$

$$\beta = \frac{2\,\mathrm{Re}}{\sqrt{3}\,|\gamma_e|}\left\{-\sqrt{\frac{32}{3}}\,FD\left[K(0,0) + \frac{3}{4}F(1,\omega_o) + \frac{9F}{32}K(0,0)\right]\right.$$

$$+ \frac{2I(I+1)aD^2}{\omega}\left[K(1,\omega_a) - \frac{4}{3}K(0,0)\right]$$

$$+ \frac{40}{21}\sqrt{\frac{2}{3}}\,I(I+1)\frac{D^3}{\omega}\left[K(0,0) - \frac{3}{4}K(1,\omega_a)\right]$$

$$\left. + \frac{5}{7}\sqrt{\frac{2}{3}}\frac{D^3}{\omega}K(1,\omega_a) - \frac{D\bar{a}^2}{\omega}K(1,\omega_a)\right\} \qquad (12b)$$

$$\gamma = \frac{2\,\mathrm{Re}}{\sqrt{3}\,|\gamma_e|}\left\{\frac{8D^2}{3}\left[K(0,0) - \frac{3}{8}K(1,\omega_a) - \frac{1}{8}K(0,\omega_o)\right.\right.$$

$$+ \frac{3}{4}K(1,\omega_o) - \frac{3}{4}K(2,\omega_o)$$

$$\left. + \frac{F}{\omega}\left(K(0,0) - \frac{15}{56}K(1,\omega_a)\right)\right]$$

$$\left. - \sqrt{\frac{8}{3}}\,\frac{FDa}{\omega}\left[K(0,0) - \frac{3}{4}K(1,\omega_a)\right]\right\} \qquad (12c)$$

$$\delta = \frac{2\,\mathrm{Re}}{\sqrt{3}\,|\gamma_e|}\left\{\frac{8}{3}\frac{D^2a}{\omega_o}\left[K(0,0) - \frac{3}{4}K(1,\omega_a)\right]\right.$$

$$\left. - \frac{64}{21}\sqrt{\frac{2}{3}}\,\frac{D^3}{\omega_o}\left[K(0,0) - \frac{15}{32}K(1,\omega_a)\right]\right\} \qquad (12d)$$

F,D,a,a" are defined as in Ref. 7; $\omega_a \simeq \frac{1}{2} a$; and ω_o is defined here as the klystron frequency.

S_z in Eq. (5) is obtained readily by[16]

$$S_z = \frac{\langle a \rangle - a'}{A_{11} - a'} \tag{13}$$

where <a> is the observed separation between hyperfine lines, A_{11} is the z principal A tensor component, and a' is the isotropic splitting corrected for nonsecular shifts.

These shifts (in gauss) are given by the formula

$$\Delta B(m,S_z) = \Delta B(m) - \frac{S_z}{\omega_x |\gamma_e|} \left\{ \frac{3}{28} F^2 + \frac{10}{21} D^2 I(I+1) + \sqrt{\frac{2}{3}} aDI(I+1) - \frac{\sqrt{6}}{7} F D m - \frac{16}{21} D^2 m^2 - \sqrt{\frac{2}{3}} aDm^2 \right\} \tag{14}$$

where $\Delta B(m)$ is the shift in an isotropic solvent.[7]

Results and Discussion

A. Magnetic Parameters

The extraction of information about molecular ordering and rotational diffusion from EPR line shapes requires that the components of the g and A tensors in the spin Hamiltonian be known. These magnetic parameters were determined from the combination of an isotropic rigid spectrum and an isotropic motionally-narrowed spectrum. The rigid isotropic spectrum was obtained by cooling the liquid crystal sample through the nematic range with the magnetic field turned off and then by recording the spectrum at 77K. A_{11} and g_{11} components are readily determined from this spectrum. The isotropic motionally narrowed spectrum was taken at 110°C, which is well above the nematic-isotropic nematic transition temperature. With the a and g_o values determined from this spectrum, $A_\perp$ and $g_\perp$ components are gotten from the equations $A_\perp = \frac{1}{2}(3a - A_{11})$ and $g_\perp = \frac{1}{2}(3g_o - g_{11})$. The magnetic parameters for VOAA were the same in both BEPC and Phase V within experimental error. The values are $A_{11} = -185 \pm 2$ G, $A_\perp = -68 \pm 1$G, $g_{11} = 1.943 \pm .001$, and $g_\perp = 1.982 \pm .001$ and are essentially those obtained in toluene.[18]

B. Motionally Narrowed Region

The approximate region where a motionally-narrowed analysis is applicable for vanadyl spin probes is indicated in Figure 1. Figure 1 is a theoretical plot of τ versus S_z where the motionally narrowed region is the area below the appropriate line. The solid line represents the breakdown of the motionally narrowed Eq. (13) for the determination of the orientational ordering parameter S_z. Only negative values for S_z were considered since typical vanadyl spin probes have $\beta_{eq} = \pi/2$ (VO bond perpendicular to the director). The dashed line indicates the breakdown of motionally narrowed line width

formula Eq. (11) for obtaining rotational dynamics. Determination of these breakdowns was made by comparison of motionally narrowed results to the general slow tumbling results (Appendix A), which are also valid in the motionally narrowed region. Calculation were for isotropic Brownian rotational diffusion ($R_{11} = R_{\perp} = \frac{1}{6\tau}$). The criteria for the lines drawn in Figure 1 are 1% deviations in the line separations and 3% deviations in the line widths from the motionally narrowed calculations. For a low degree of ordering, these deviations begin to occur in the high-field outside hyperfine lines. For high degree of ordering, deviations occur initially in the central lines. VOAA magnetic parameters were used in these calculations. Slight differences in Figure 1 would result from using magnetic parameters of other vanadyl spin probes. Also, rotational diffusion other than the isotropic Brownian model would show slight discrepencies from that given in Figure 1. The use of Figure 1 presumes a recognition of the sensitivity of EPR spectral line shapes to changes in τ and $\lambda(S_z)$. When the vanadyl spin probe is highly ordered, the EPR spectrum will naturally become less sensitive to rotational diffusion and ordering potential changes. Such changes, in practice, may be camouflaged by an orientation-independent line width $\alpha''(T_2^{-1})$, which may be regarded as a resolution parameter.

C. Slow Tumbling EPR Line Shapes

Experimental EPR spectra for VOAA were recorded in the nematic range from 82°C to 37°C for BEPC and from 72°C to -29°C for Phase V. Figures 2-4 show typical experimental spectra that are both near the isotropic-nematic transition temperature T_K and reasonably near to the nematic-solid transition temperature. Simulated spectra calculated from equations in either Appendix A or Appendix B are presented as broken lines. All experimental spectra

formula Eq. (11) for obtaining rotational dynamics. Determination of these breakdowns was made by comparison of motionally narrowed results to the general slow tumbling results (Appendix A), which are also valid in the motionally narrowed region. Calculation were for isotropic Brownian rotational diffusion ($R_{11} = R_{\perp} = \frac{1}{6\tau}$). The criteria for the lines drawn in Figure 1 are 1% deviations in the line separations and 3% deviations in the line widths from the motionally narrowed calculations. For a low degree of ordering, these deviations begin to occur in the high-field outside hyperfine lines. For high degree of ordering, deviations occur initially in the central lines. VOAA magnetic parameters were used in these calculations. Slight differences in Figure 1 would result from using magnetic parameters of other vanadyl spin probes. Also, rotational diffusion other than the isotropic Brownian model would show slight discrepencies from that given in Figure 1. The use of Figure 1 presumes a recognition of the sensitivity of EPR spectral line shapes to changes in τ and $\lambda(S_z)$. When the vanadyl spin probe is highly ordered, the EPR spectrum will naturally become less sensitive to rotational diffusion and ordering potential changes. Such changes, in practice, may be camouflaged by an orientation-independent line width $\alpha''(T_2^{-1})$, which may be regarded as a resolution parameter.

C. Slow Tumbling EPR Line Shapes

Experimental EPR spectra for VOAA were recorded in the nematic range from 82°C to 37°C for BEPC and from 72°C to -29°C for Phase V. Figures 2-4 show typical experimental spectra that are both near the isotropic-nematic transition temperature T_K and reasonably near to the nematic-solid transition temperature. Simulated spectra calculated from equations in either Appendix A or Appendix B are presented as broken lines. All experimental spectra

taken in the nematic range clearly exhibited the eight hyperfine line spectrum indicative of motional averaging. These line shapes suggest that there should be enough rotational motion about the VO bond to average out the small magnetic anisotropy in the x and y principal axes. Subsequent analysis bears this out. Thus the use of axially symmetric magnetic parameters and of Eq. (2) for the restoring potential is felt to be well justified. All spectra in the nematic range had highly asymmetric lines which are very suggestive of slow tumbling effects. In fact, spectra in the isotropic phase just above the isotropic-nematic transition temperature T_k were obviously in the slow tumbling region. Although there was considerably supercooling below the nematic-solid freezing point, no discontinuities were observed in the EPR spectra or in their subsequent analysis. Both the observed isotropic-nematic and observed nematic-solid transition temperatures were clearly discerned by dramatic changes is the EPR spectra.

The computer simulations for the slow tumbling EPR line shapes are calculated by the method developed by PBF[13](See Appendix A for the explicit equations that were used) or by a modified version[10](See Appendix B).

Fiquire 2 shows the experimental spectrum for VOAA in BEPC at 79°C, which is just below the T_k. Simulated spectra, that are calculated for Brownian rotational diffusion (Appendix A), are also shown. Spectra for isotropic Brownian rotation are simulated by varying essentially only two parameters, τ and λ. The general effects of varying τ and λ on spectral line shapes are given in PBF[13]. Note that for vanadyl spin probes, which have $\lambda < 0$ and $|A_\perp| < |A_{11}|$, the effects of slow tumbling is to shift intensity of the

hyperfine lines closer together. Thus a motionally narrowed analysis, which would ascribe such shifts to an increased ordering (λ more negative) rather than to a longer τ, overestimates the degree of ordering for the slow tumbling region. Figure 2 is a typical best fit of an isotropic Brownian rotational diffusion model to an experimental VOAA EPR spectrum. Although significant discrepencies are indicated, the estimated best fit S_z and τ values are reasonable and represent a significant improvement over a motionally narrowed analysis. Improved fits to the experimental spectra were made by introducing an anisotropic viscosity ($R_{11} \neq R_\perp$). Spectral simulation for this model were fit by varying essentially three parameters (τ_{11}, $\tau_\perp$, and λ). Figure 2 shows the improved agreement with $\tau_\perp \approx 8\tau_{11}$. However, the ratio $\tau_\perp/\tau_{11}$ increases rapidly and τ_{11} becomes shorter with decreasing temperatures. Similar implausible results for nitroxide probes have been reported by Polnaszek and Freed,[10] who then invoked a slowly flucuating torque analysis.

Such an analysis is expected to be appropriate here because of the small size of VOAA relative to the ordered liquid crystalline solvating molecules. Figures 3 and 4 show spectral fits which are based upon this analysis (Appendix B). For purposes of comparison to nitroxide spin probe studies, only two correction factors, ϵ'_{sec} and ϵ'_{psec}, to spectral density functions will be considered. Note $\epsilon' = 1$ yields Brownian diffusion results while $\epsilon' > 1$ indicates deviations from Brownian diffusion. Also we let $R_{11}(0) = R_\perp(0) = \frac{1}{6\tau}$. The intention of this analysis is to establish a set of ϵ' values for all temperatures in the nematic range. With ϵ' values fixed, spectral fits are made by varying two parameters, τ and λ. The values $\epsilon'_{sec} = 1.5 \pm 0.5$ and $\epsilon'_{psec} = 10 \pm 2$ would appear to be a consistent set of parameters except for a ~15°C temperature range below the T_K. (See Figures 3 and 4.) For

this temperature range, $\varepsilon'_{psec} = 4 \pm 2$ gave better fits. Although some systematic discrepencies between calculated and experimental spectra still exist, the spectral fits were good. This analysis gave τ values that were precise to ≈10% except for low temperatures in Phase V where the precision was ≈20%. S_z values computed numerically from λ (See Eq. 3) were precise to ≈5%.

The τ and S_z values determined from these best fitting spectra, which incorporated the ε' corrections, are used in Figures 5 and 6. Figure 5 is a plot of S_z versus temperature (T) where S_z is calculated numerically from Eq. 3. A plot of log τ versus $\frac{1}{T}$ is shown in Figure 6. With the neglect of a ≈15°C temperature range below T_k, Figure 6 for Phase V shows good Arrhenius behavior with an activation energy of 9.0 ± 0.4 kcal/mole. This value is comparable to that found for nitroxide spin probes.[10,29,30] The pre-exponential factor is $(3.4\pm1.1)\times10^{-16}$ sec/rad. BEPC had too short of a nematic range to determine accurate Arrhenius parameters.

Attempts to account for the deviation from Brownian rotation by invoking a static distribution of director orientations were not successful. Here, a line shape $g(\Delta\omega,\phi_o)$ was calculated by the summation (i.e., a trapezoidal rule) of spectral amplitudes $f(\Delta\omega,\phi)$ weighed by the distribution factor $\exp(-\sin^2\phi/\phi_o^2)\sin\phi$ where ϕ is the angle between the director and the external magnetic field.[10,32] ϕ_o is the root mean square deviation (spread) in ϕ. In particular, the experimental spectrum for VOAA in BEPC at 79°C was used. For Brownian rotation with $\tau = 4.1 \times 10^{-10}$ sec/rad, $S_z = -0.13$, and $\phi_o = 0.17$ rad (10°); the calculated line shape $g(\Delta\omega,\phi_o)$ showed a change in asymmetry of the hyperfine lines opposite to that which is observed.

Director flucuations are predicted to have neglible effects on the EPR spectra of the relatively small VOAA probe.[10] Also, a simple jump model of rotational reorientation was inadequate to explain the discrepencies from Brownian rotational diffusion.

Conclusion

This work is an initial inquiry of slowly tumbling vanadyl spin probes in an anisotropic medium. Here the stochastic Liouville method as developed by PBF[13] has been appropriately applied to the analysis of EPR spectra from VOAA in viscous nematic liquid crystals. The use of vanadyl complexes as spin probes for nematic liquid crystals greatly simplifies theoretical calculations and interpretation. Guide lines for the breakdown of motionally narrowed formulas were established (see Figure 1).

Spectral simulations for experimental spectra of VOAA in nematic BEPC and Phase V showed that VOAA was in the slow tumbling region throughout the nematic range of both these viscous solvents. Also, deviations from Brownian rotation were noted. An analysis, in which inertial effects on the probe reorientation are induced by slowly flucuating torque components of the local solvent structure, results in improved spectral fits. Such an analysis, which introduces correction factors ϵ'_{sec} and ϵ'_{psec}, yields quantitative values for τ and S_z. τ values for the weakly ordered VOAA showed relatively little variation with temperature near the isotropic-nematic transition temperature T_K. (See Figure 6.) Here, $\epsilon'_{sec} = 1.5 \pm 0.5$ and $\epsilon'_{psec} = 4 \pm 2$ gave good spectral fits. For temperatures more than 15°C below T_K, τ showed good Arrhenius behavior with an activation energy of 9.0 ± 0.4 kcal/mole in Phase V. Here $\epsilon'_{sec} = 1.5 \pm 0.5$ and $\epsilon'_{psec} = 10 \pm 2$ gave good spectral fits. These

results suggest that nematogens undergo orientational flucuations over a reasonably wide temperature range near T_K that are different from the flucuations that may occur far below T_K. Our studies indicate that vanadyl complexes may be good probes for the study of phenomena near T_K. Specifically, VOAA was obviously in the slow tumbling region, where EPR spectra are most sensitive to motional dynamics, at T_K of BEPC and Phase V.

In their detailed study with the small nitroxide spin probe PD-tempone, Polnaszek and Freed[10] introduced a slowly flucuating torque analysis to account for "anomolous" EPR line shapes. In particular, values of ε'_{sec} = 1-2 and ε'_{psec} = 15-20 were used in the incipient slow tumbling region ($T < -6°C$) in Phase V. Results for VOAA in this region show similar effects but with smaller ε' values. This difference may be attributed to a larger effective rotational radius for VOAA. However, our results indicate slowly flucuating torque effects throughout the nematic range but much reduced near T_K. Other comparisons show that VOAA exhibits behavior similar to that of PD-tempone. VOAA is slighly more ordered and it reorients more slowly with roughly the same activation energy.[10]

In summary, our results indicate that both the slow tumbling aspects and the effects of non-Brownian rotation should be resolved in order to extract quantitative information about molecular ordering and rotational mobility. This present study should not be considered a critique of the slowly flucuating torque analysis. The work here does show that, effects which were observed for PD-tempone, are also seen for the commonly used probe VOAA. Undoubtably, the slowly flucuating torque analysis does provide a proper framework for explaining such effects. Further work is needed to characterize the correction factor ε' (e.g. different size and shape probes). Refined theory and develop-

ment of other techniques of solution should yield a clearer and more precise explanation for the motional dynamics of the spin probe. Because of the present necessary simplification in theory,[10,29] inclusion of other effects (e.g., director distribution and flucuation, anisotropic viscosity) into the slowly flucuating torque analysis were not justified.

Acknowledgement

We are grateful for the generous use of the computer facilities provided by the University of Texas at El Paso. Discussions with Dr. C. F. Polnaszek about the slowly flucuating torque analysis are greatly appreciated. This research was supported by NASA Grant NSG-1316 and by the Robert A. Welch Foundation of Houston, Texas.

Appendix A

This appendix indicates explicitly the equations that were used for obtaining vanadyl EPR line shapes for Brownian rotational diffusion with an anisotropic viscosity (Eq. 8) under a simple one term Maier-Saupe restoring potential (Eq. 2). These equations may be obtained most easily by modification of the isotropic liquid equations,[13] which are explicitly given by Eq. A.1 - A.4, B.3 of Ref. 7. The following term is added to the left-hand side of Eq. A.1 - A.3 in Ref. 7:

$$-i[(R_{11} - R_\perp)n^2 + \frac{2}{15} R_\perp \lambda^2]C^L_{o,n}(j)$$

$$+ i2 R_\perp \lambda(1 - \frac{\lambda}{21})(-1)^n \sum_{L'} N(L,L')\begin{pmatrix} L & 4 & L' \\ 0 & 0 & 0 \end{pmatrix}\begin{pmatrix} L & 2 & L' \\ -n & 0 & n \end{pmatrix} C^{L'}_{o,n}(j)$$

$$+ i \frac{8}{35} R_\perp \lambda^2(-1)^n \sum_{L'} N(L,L')\begin{pmatrix} L & 4 & L' \\ 0 & 0 & 0 \end{pmatrix}\begin{pmatrix} L & 4 & L' \\ -n & 0 & n \end{pmatrix} C^{L'}_{o,n}(j) \quad (A.1)$$

The right hand side of Eq. A.1 of Ref. 7 becomes

$$u_L = [\frac{2L + 1}{I_o}]^{1/2} \int_o^\pi D^L_{o,o}(o,\theta,o)\exp[\frac{1}{2}\lambda \cos^2\theta]\sin\theta d\theta \quad (A.2)$$

where I_o is

$$I_o = \int_o^\pi \exp(\frac{1}{2}\lambda \cos^2\theta)\sin\theta d\theta \quad (A.3)$$

The absorption Z" in Eq. (A.4) of Ref.7 now becomes

$$Z'' = \mathrm{Im} \sum_{L'} \sum_{m=-I}^{I} u_L C^L_{o,o}(2m + 2I + 2, 2m + 2I + 1) \quad (A.4)$$

Contributions from nonsecular terms in addition to those given by expression B.3 in Ref. 7 have been included. Here, nonsecular corrections to the "forbidden" transition terms have been made. Nonsecular contributions to the coupling $C^{L}_{0,0}(i) \rightarrow C^{L\pm4}_{0,0,}(i)$ for allowed transitions, which are made significant by Eq. (A.1), have also been included. These nonsecular contributions are obtained by straightforward application of previous perturbation analysis.[7,13] The results for the coupling to the $\bar{C}^{L}_{0,n}(a,b;c,d)$ transition terms are given by the expression

$$
\begin{aligned}
(-1)^{n+1}\,\frac{1}{\omega}\Bigg[& \left\{ \frac{3F^2}{20} - \frac{\sqrt{6}}{5}(m+n)FD + \frac{D^2}{30}\left[14I(I+1) - 2m^2 - 2nm - n^2\right] \right. \\
& \left. + \frac{a^2}{4}\left[2I(I+1) - 2m^2 - 2nm - n^2\right] \right\} \bar{C}^{L}_{0,n}(a,b;c,d) \\
+ & \sum_{L'} N(L,L') \left\{ \frac{3F^2}{28} - \frac{\sqrt{6}}{7}\left(m+\frac{n}{2}\right)FD + \frac{D^2}{21}\left[-10I(I+1) + 16m^2 + 16nm \right.\right. \\
& \left.\left. + 8n^2\right] + \frac{aD}{\sqrt{6}}\left[-2I(I+1) + 2m^2 + 2nm + n^2\right] \right\} \begin{pmatrix} L & 2 & L' \\ 0 & 0 & 0 \end{pmatrix} \begin{pmatrix} L & 2 & L' \\ -n & 0 & n \end{pmatrix} \bar{C}^{L'}_{0,n}(a,b;c,d) \\
+ & \sum_{L'} N(L,L') \left\{ -\frac{9F^2}{35} + \frac{12\sqrt{6}}{35}\left(m+\frac{n}{2}\right)FD + \frac{D^2}{35}\left[12I(I+1) - 36m^2 \right.\right. \\
& \left.\left. - 36nm - 18n^2\right] \right\} \begin{pmatrix} L & 4 & L' \\ 0 & 0 & 0 \end{pmatrix} \begin{pmatrix} L & 4 & L' \\ -n & 0 & n \end{pmatrix} \bar{C}^{L'}_{0,n}(a,b;c,d) \\
+ & \sum_{L'} N(L,L') f(I,m+n) \left[-\frac{5FD}{28} + \frac{\sqrt{6}}{84}(10m + 10n + 5)D^2 - \frac{\sqrt{6}aF}{8} \right. \\
& \left. + \frac{(2m + 2n + 1)aD}{4} \right] \begin{pmatrix} L & 2 & L' \\ 0 & 0 & 0 \end{pmatrix} \begin{pmatrix} L & 2 & L' \\ -n & -1 & n+1 \end{pmatrix} \bar{C}^{L'}_{0,n+1}(a+1,b;c,d+1) \\
+ & \sum_{L'} N(L,L') f(I,m+n) \left[\frac{3\sqrt{30}FD}{70} - \frac{3\sqrt{5}}{35}(2m + 2n + 1)D^2 \right] \times \\
& \times \begin{pmatrix} L & 4 & L' \\ 0 & 0 & 0 \end{pmatrix} \begin{pmatrix} L & 4 & L' \\ -n & -1 & n+1 \end{pmatrix} \bar{C}^{L'}_{0,n+1}(a+1,b;c,d+1) \\
+ & \sum_{L'} N(L,L') f(I,m-1) \left[-\frac{5FD}{28} + \frac{\sqrt{6}}{42}(10m - 5)D^2 - \frac{\sqrt{6}aF}{8} \right. \\
& \left. + \frac{(2m - 1)aD}{4} \right] \begin{pmatrix} L & 2 & L' \\ 0 & 0 & 0 \end{pmatrix} \begin{pmatrix} L & 2 & L' \\ -n & -1 & n+1 \end{pmatrix} \bar{C}^{L'}_{0,n+1}(a,b-1;c-1,d)
\end{aligned}
$$

$$+ \sum_{L'} N(L,L')f(I,m-1)\left[\frac{3\sqrt{30}FD}{70} - \frac{3\sqrt{5}(2m-1)D^2}{35}\right]\begin{pmatrix} L & 4 & L' \\ 0 & 0 & 0 \end{pmatrix}\begin{pmatrix} L & 4 & L' \\ -n & -1 & n+1 \end{pmatrix}\bar{C}^{L'}_{0,n+1}(a,b-1;c-1,d)$$

$$+ \sum_{L'} N(L,L')f(I,m+n-1)\left[\frac{5FD}{28} - \frac{\sqrt{6}(10m+10n-5)D^2}{84} + \frac{\sqrt{6}aF}{8}\right.$$

$$\left. - \frac{(2m+2n-1)aD}{4}\right]\begin{pmatrix} L & 2 & L' \\ 0 & 0 & 0 \end{pmatrix}\begin{pmatrix} L & 2 & L' \\ -n & 1 & n-1 \end{pmatrix}\bar{C}^{L'}_{0,n-1}(a-1,b;c,d-1)$$

$$+ \sum_{L'} N(L,L')f(I,m+n-1)\left[-\frac{3\sqrt{30}FD}{70} + \frac{3\sqrt{5}(2m+2n-1)D^2}{35}\right] x$$

$$x \begin{pmatrix} L & 4 & L' \\ 0 & 0 & 0 \end{pmatrix}\begin{pmatrix} L & 4 & L' \\ -n & 1 & n-1 \end{pmatrix}\bar{C}^{L'}_{0,n-1}(a-1,b;c,d-1)$$

$$+ \sum_{L'} N(L,L')f(I,m)\left[\frac{5FD}{28} - \frac{\sqrt{6}(10m+5)D^2}{84} + \frac{\sqrt{6}aF}{8}\right.$$

$$\left. - \frac{(2m+1)aD}{4}\right]\begin{pmatrix} L & 2 & L' \\ 0 & 0 & 0 \end{pmatrix}\begin{pmatrix} L & 2 & L' \\ -n & 1 & n-1 \end{pmatrix}\bar{C}^{L'}_{0,n-1}(a,b+1;c+1,d)$$

$$+ \sum_{L'} N(L,L')f(I,m)\left[-\frac{3\sqrt{30}FD}{70} + \frac{3\sqrt{5}(2m+1)D^2}{35}\right] x$$

$$x \begin{pmatrix} L & 4 & L' \\ 0 & 0 & 0 \end{pmatrix}\begin{pmatrix} L & 4 & L' \\ -n & 1 & n-1 \end{pmatrix}\bar{C}^{L'}_{0,n-1}(a,b+1;c+1,d) \qquad (A.5)$$

The above expression (A.5) is added to the left hand side of Eq.(A.3) in Ref. 7. Eq.(A.2) in Ref. 7 may be regarded as a special case of Eq.(A.3) in Ref. 7. Expression (A.5) was also used for the additional nonsecular coupling to the allowed transition terms. In the derivation of expression (A.5), $R \ll \omega$. Also, within second order perturbation theory, the nonsecular coupling couplings $\bar{\varepsilon}^{L'}_{0,n'}(k)$ between $\bar{C}^{L}_{0,n}(i)$ and $\bar{C}^{L'}_{0,n'}(k)$ were approximated by the equations

$$\bar{\varepsilon}^{L'}_{0,n} = \frac{1}{2}\left(\varepsilon^{L'}_{0,n} + \varepsilon^{L'}_{0,-n}\right) \qquad (A.6a)$$

and

$$\bar{\varepsilon}^{L'}_{0,n\pm1} = \frac{1}{2}\left(\varepsilon^{L'}_{0,n\pm1} - \varepsilon^{L'}_{0,-(n\pm1)}\right) \qquad (A.6b)$$

Note that for $n=0$, $\bar{C}^{L}_{0,0} = \sqrt{2}C^{L}_{0,0}$ and $\bar{\varepsilon}^{L}_{0,1} \rightarrow \sqrt{2}\bar{\varepsilon}^{L}_{0,1}$.

To summarize, the equations which were used are obtained from Eqs. (A.1-A.3) in Ref. 7 that have been modified by (B.3) of Ref. 7, (A.1-A.3), and (A.5). Eq. (A.4) yields the absorption line shape. Eqs. (A.2) and (A.3) are solved numerically with recursion relations.[12] The first derivative EPR line shapes are then most efficiently obtained by a diagonalization method.[33,34]

Appendix B

Details for explicitly obtaining slowly flucuating torque effects in the EPR line shapes is given by Polnaszek.[29] The general expression way be written

$$(\omega - \omega_j - iq\,\tau_q^{-1})\, C^n_{o,m,p,q}(j) + \sum_{n',m'} \langle u^n_{o,m} | [H_1(\Omega),\, C^{n'}_{o,m',p,q} | u^{n'}_{o,m'} \rangle$$

$$+ \left(\frac{E^n_{o,m}}{R} \frac{kT}{I} \right)^{1/2} [\sqrt{p+1}\, C^n_{o,m,p+1,q}(j) + \sqrt{p}\, C^n_{m,p-1,q}(j)]$$

$$+ \left[\frac{1}{R\tau_q} \frac{kT}{I} \right]^{1/2} [\sqrt{p}\,\sqrt{q+1}\, C^n_{o,m,p-1,q+1}(j) + \sqrt{p+1}\,\sqrt{q}\, C^n_{o,m,p+1,q-1}(j)]$$

$$= \delta_{no}\,\delta_{mo}\,\delta_{po}\,\delta_{qo} \qquad \text{B.1}$$

where $\tau_q = \dfrac{\sqrt{\epsilon'} - 1}{6R}$ B.2

and τ_q represents a correlation time for the decay of the nertial effects induced by the solvent. To include effects induced by torque components parallel and perpendicular to a director of a nematic liquid crystal solvent, ϵ' may be labeled ϵ'_{sec} and ϵ'_{psec} to express these parallel and perpendicular components, respectively. Note that for $\epsilon' \to 1$, Brownian rotational diffusion is obtained. $\epsilon' > 1$ indicate deviations from Brownian rotation.

Eq. (B.1) has only $p = 0$, $q = 0$; $p = 1$, $q = 0$; and $p = 0$, $q = 1$ combinations for the lowest order inertial effects. Note that the eigenfunctions $u^n_{o,m}$ and eigenvalues $E^n_{o,m}$ are used (Eq. 9).

The procedure to obtain the equations used for the slowly flucuating torque analysis may be summarized in three steps. First, diagonalize the rotational diffusion operator (Eq. 8) to obtain $u^n_{0,m}$ and $E^n_{0,m}$. (See Eq. 9.)

The real symmetric rotational diffusion matrix (Eq. 8) may be blocked according to different m values and each block may be numerically diagonalized separately. Second, perform a similarity transformation on the matrix formed from the coefficients of the transition terms $C^{L}_{0,n}$ developed in Appendix A. Retain only those terms that have F or D in them. The columns of the similarity transformation post-matrix are the vectors whose components are the coefficients $a^{(n)L}_{0,m}$ in Eq. 9a. This step calculates the summation(second term) on the left hand side of Eq. B.1. Third, form the entire matrix by using Eq. B.1. This matrix may be viewed as partitioned into three sections according to the three combinations of p,q that were used.

The absorption line shape Z'' is then given by the following

$$Z'' = \mathrm{Im} \sum_{m=-I}^{I} C^{0}_{0,0,0,0}{}^{(2m+2I+2,\,2m+2I+1)} \quad . \qquad \text{B.3}$$

First derivative EPR line shapes are efficiently calculated by numerical diagonalization method.[33,34]

References

1. "Spin Labeling: Theory and Application", L. Berliner, Ed., Academic Press, New York, N. Y.,1976.

2. "Spin Labeling", G. T. Likhtenstein, Ed., Navka, Moscow, USSR (1974).

3. (a) D. Hoel and D. Kivelson, J. Chem. Phys. 62, 4535 (1975)

   (b) J. S. Hwang, D. Kivelson, and W. Z. Placky, J. Chem. Phys. 58, 1753 (1973).

4. (a) G. R. Luckhurst, "ESR Relaxation in Liquids", L. T. Muns and P. W. Atkins, Ed. Plenum Press, New York, N. Y., 1972, Chapter XV.

   (b) G. R. Luckhurst, "Liquid Crystals and Plastic Crystals", Vol. 2, G. W. Gray and P. A. Winsor, Ed. Ellis Horwood, New York, N. Y., 1974, Chapter 7.

5. (a) N. D. Chasteen, R. J. De Koch, B. Rodgers, and M. W. Hanna, J. Am. Chem. Soc., 95, 1301 (1973).

   (b) R. J. De Koch, D. J. West, J. C. Cannon, and N. D. Chasteen, Biochemistry, 13, 4347 (1974).

   (c) N. D. Chasteen and J. J. Fitzgerald, ibid., 13, 4338 (1974).

6. R. F. Campbell and M. W. Hanna, J. Phys. Chem. 80, 1892 (1976).

7. G. V. Bruno, J. K. Harrington, and M. P. Eastman, J. Phys. Chem. 81, 1111 (1977).

8. G. C. Fryburg and E. Gelerinter, J. Chem. Phys. 52, 3378 (1970).

9. J. I. Kaplan, E. Gelerinter, and G. C. Fryburg, Mol. Cryst. Liq. Cryst. 23, 69 (1973).

10. C. F. Polnaszek and J. H. Freed, J. Phys. Chem. 79, 2283 (1975).

11. S. H. Glarum and J. H. Marshall, (a) J. Chem. Phys. 44, 2884 (1966); (b) J. Chem. Phys. 46, 55 (1967).

12. (a) P. L. Nordio and P. Busolin, J. Chem. Phys. 55, 5485 (1971);

    (b) P. L. Nordio, G. Rigatti, and U. Segre, J. Chem. Phys. 56, 2117 (1972).

13. C. F. Polnaszek, G. V. Bruno, and J. H. Freed, J. Chem. Phys. 58, 3185 (1973).

14. "Introduction to Liquid Crystals", E. B. Priestley, P. J. Wojtowicz, P. Sheng, Ed., Plenum Press, New York, N. Y. 1974.

15. N. D. Chasteen and M. W. Hanna, J. Phys. Chem., 76, 3951 (1972).

16. N. M. Atherton, "Electron Spin Resonance", Ellis Horwood, Chichester, 1973.

17. J. H. Freed, G. V. Bruno, and C. F. Polnaszek, J. Phys. Chem. 75, 3385 (1971).

18. R. Wilson and D. Kivelson, J. Chem. Phys. 44, 154 (1966).

19. B. E. Bryant and W. C. Fernelius, Inorg. Syn. 5, 115 (1957).

20. R. Kubo, "Stochostic Processes in Chem. Phys. Advances in Chemical Physics", Vol. XVI, K. E. Shaler, Ed., Wiley, New York, N. Y., 1969.

21. B. F. Campbell (private communication).

22. P. G. James and G. R. Luckhurst, Mol. Phys. 19, 489 (1970).

23. (a) W. Maier and A. Saupe, Z. Naturforsch 13a, 564 (1958).

(b) W. Maier and A. Saupe, Z. Naturforsch 14a, 882 (1959).

24. M. Rotenberg, R. Bivins, N. Metropolis, and J. K. Wooten, "The 3j and 6j Symbols", Technology Press, M. I. T., 1959.

25. G. R. Luckhurst, Physics Bull. 23, 279 (1972).

26. G. V. Bruno and J. H. Freed, J. Phys. Chem. 78, 935 (1974).

27. L. P. Hwang and J. H. Freed, J. Chem. Phys. 63, 118 (1975).

28. J. S. Hwang, R. P. Mason, L. P. Hwang, and J. H. Freed, J. Phys. Chem. 79, 489 (1975).

29. C. F. Polnaszek, Ph.D. Thesis, Cornell University, Ithaca, N. Y. (1976).

30. K. V. S. Rao, C. F. Polnaszek, and J. H. Freed, J. Phys. Chem. 81, 449 (1977).

31. I. Zupancic, M. Vilfan, M. Sentjurc, M. Schora, F. Pusnik, J. Pers, and R. Bline, "Liquid Crystals and Ordered Fluids" Vol. 2, G. H. Brown, Ed., Plenum Press, New York, N. Y. 1974. p. 525.

32. S. A. Brooks, G. R. Luckhurst, and G. F. Pedulli, Chem. Phys. Lett. 11, 159 (1971).

33. G. V. Bruno, Ph.D. Thesis, Cornell University, Ithaca, N. Y. (1973).

34. R. G. Gordon and T. Messinger, "ESR Relaxation in Liquids", L. T. Muses and P. W. Atkins, Ed., Plenum Press, New York, N. Y. 1972, Chapt. XIII.

Figure Captions

Figure 1. Graph of rotational correlation time τ versus ordering parameter S_z for the breakdown of motionally narrowed formulae. (——) is breakdown for line separations; (---) is breakdown for line widths. Calculations were made for isotropic Brownian rotation with simple one-term Maier-Saupe restoring potential. VOAA magnetic parameters were used.

Figure 2. A comparison of simulated and experimental spectra for VOAA in BEPC at 79°C. (——) is experimental spectrum. (---) is calculated for isotropic Brownian rotation with $\tau = 4.1 \times 10^{-10}$ sec/rad and $S_z = -0.13$. (····) is calculated for Brownian rotation and anisotropic viscosity with $\tau_\perp = 4.1 \times 10^{-10}$ sec/rad, $\tau_{11} = 5.1 \times 10^{-11}$ sec/rad, and $S_z = -0.13$.

Figure 3. Comparison of simulated and experimental spectra for VOAA in BEPC at 79°C and 38°C. (——) are experimental spectra. (---) are calculated with $\varepsilon'_{sec} = 1.5$, $\varepsilon'_{psec} = 4$. (····) are calculated with $\varepsilon'_{sec} = 1.5$, $\varepsilon'_{psec} = 10$. At 79°C, $\tau = 4.1 \times 10^{-10}$ sec/rad, $S_z = -0.13$; at 38°C, $\tau = 1.7 \times 10^{-9}$ sec/rad, $S_z = -0.21$.

Figure 4. Comparison of simulated and experimental spectra for VOAA in Phase V at 69°C and 0°C. (——) are experimental spectra. (---) are calculated with $\varepsilon'_{sec} = 1.5$, $\varepsilon'_{psec} = 4$. (····) are calculated with $\varepsilon'_{sec} = 1.5$, $\varepsilon'_{psec} = 10$. At 69°C, $\tau = 2.6 \times 10^{-10}$ s/rad, $S_z = -0.103$; at 0°C, $\tau = 5.9 \times 10^{-9}$ sec/rad, $S_z = -0.22$.

Figure 5. Graph of ordering parameter S_z versus temperature T for VOAA in Phase V (● - ϵ'_{psec}=10; ○ - ϵ'_{psec}= 4) and BEPC (▲ - ϵ'_{psec}= 10; Δ - ϵ'_{psec}= 4). Solid line is drawn for Phase V and dashed line is for BEPC. ϵ'_{sec}= 1.5.

Figure 6. Graph of rotational correlation time τ(sec/rad) versus $\frac{1}{T}$ for VOAA in Phase V (● - ϵ'_{psec}= 10; ○ - ϵ'_{psec}= 4) and BEPC (▲ - ϵ'_{psec}=10; Δ - ϵ'_{psec}= 4). Solid line is drawn for Phase V and dashed line is for BEPC. ϵ'_{sec}= 1.5.

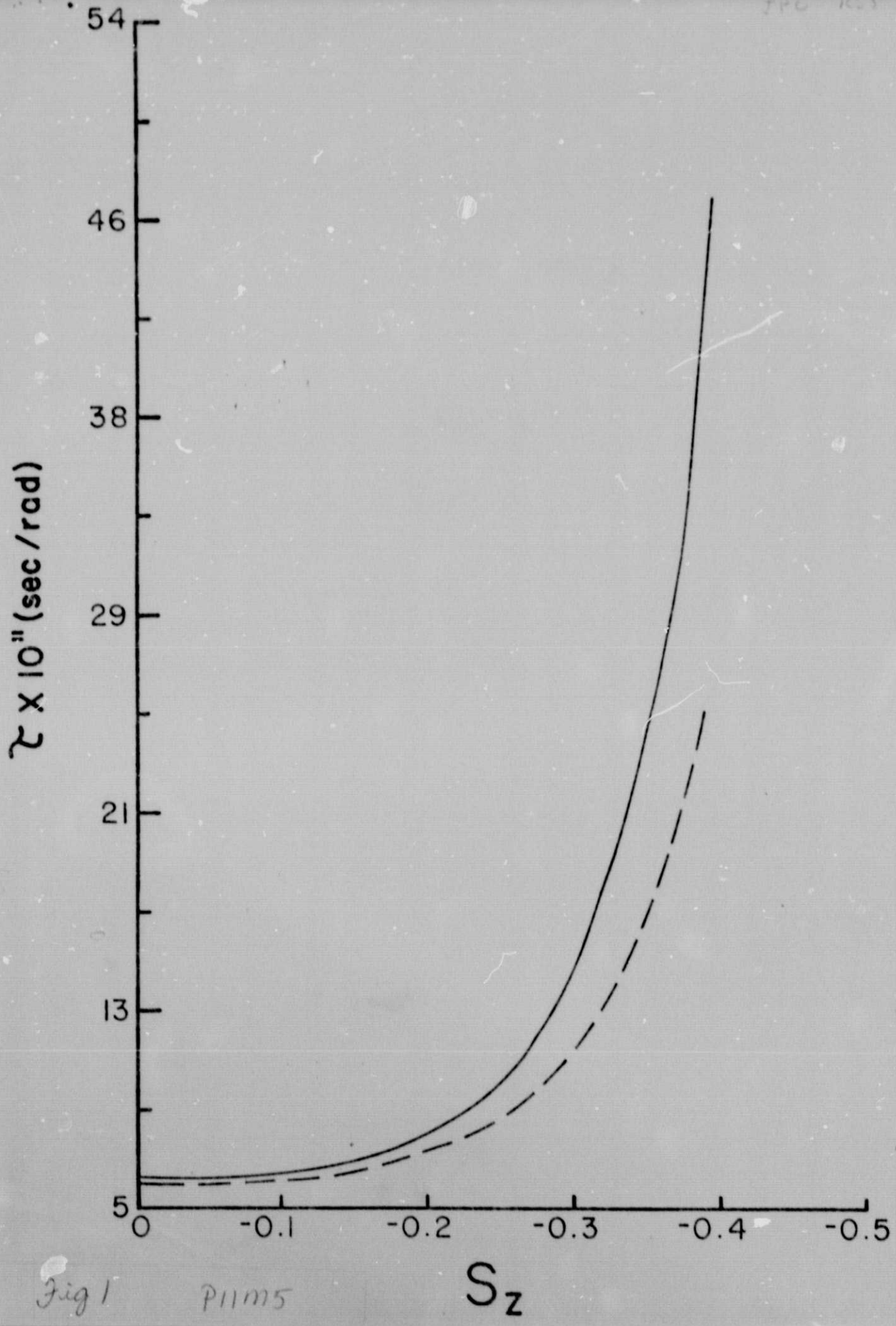

Fig 1 P11M5

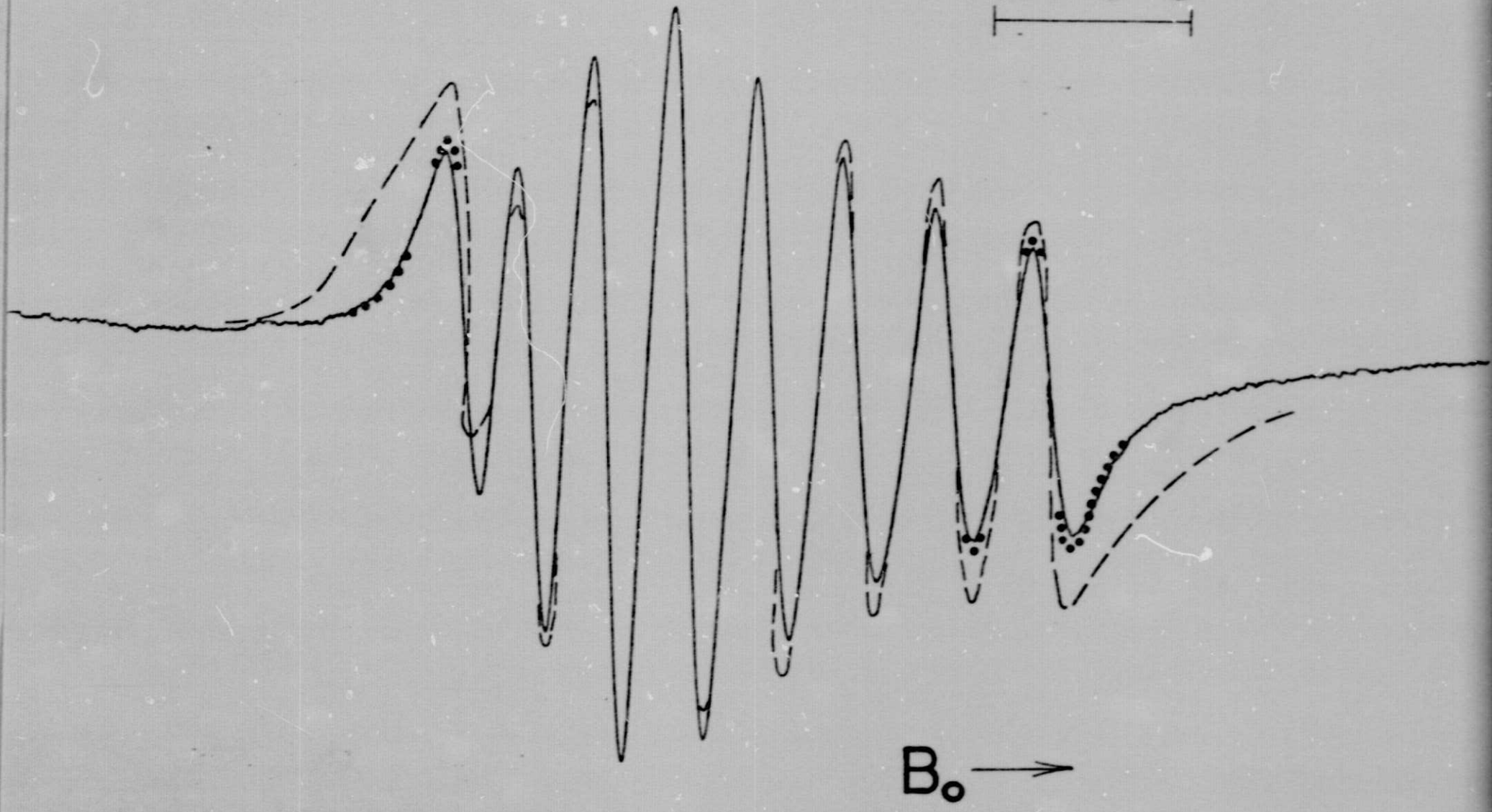

Fig 2 PIIMS

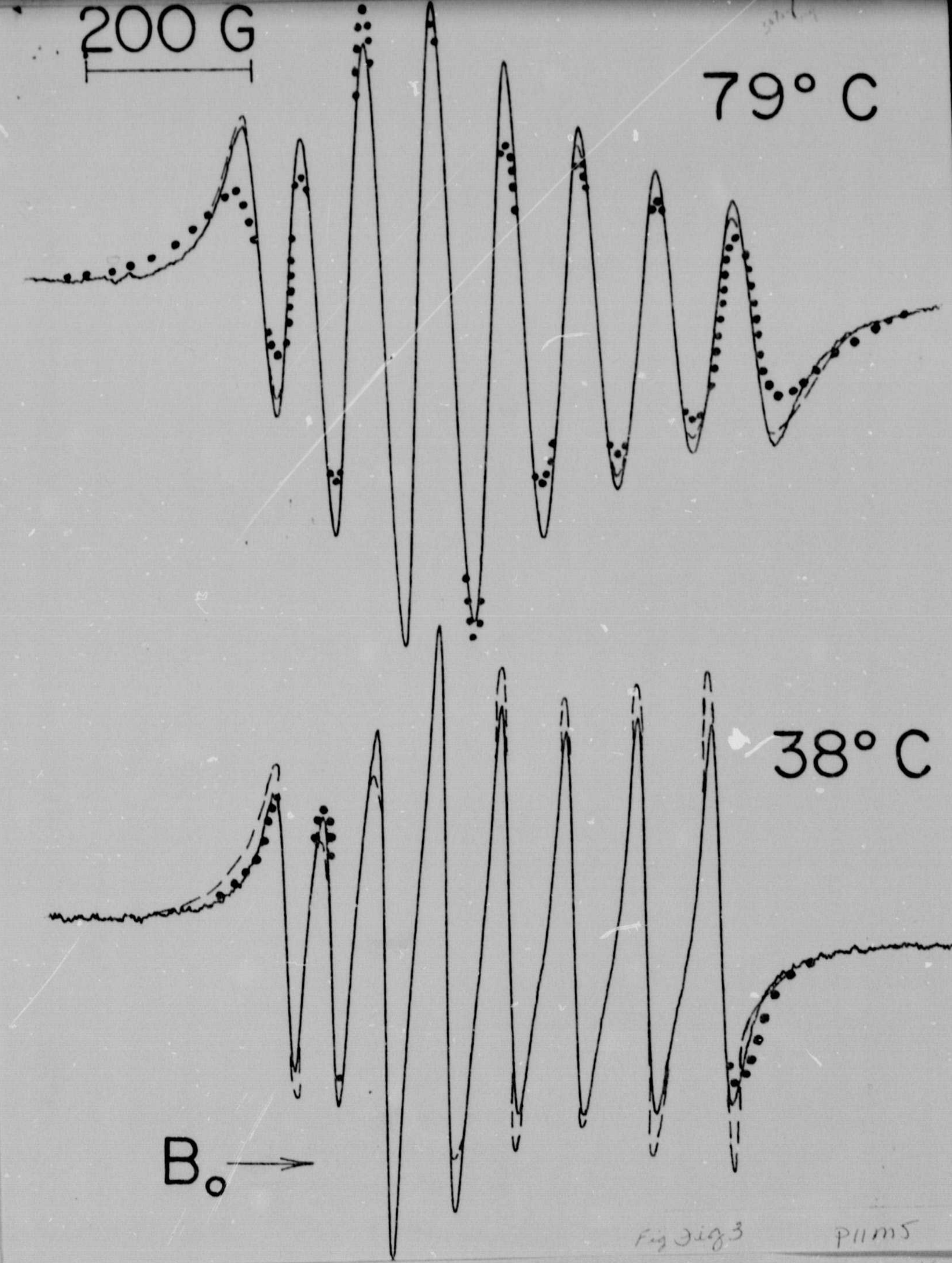
200 G
79° C
38° C
B_o

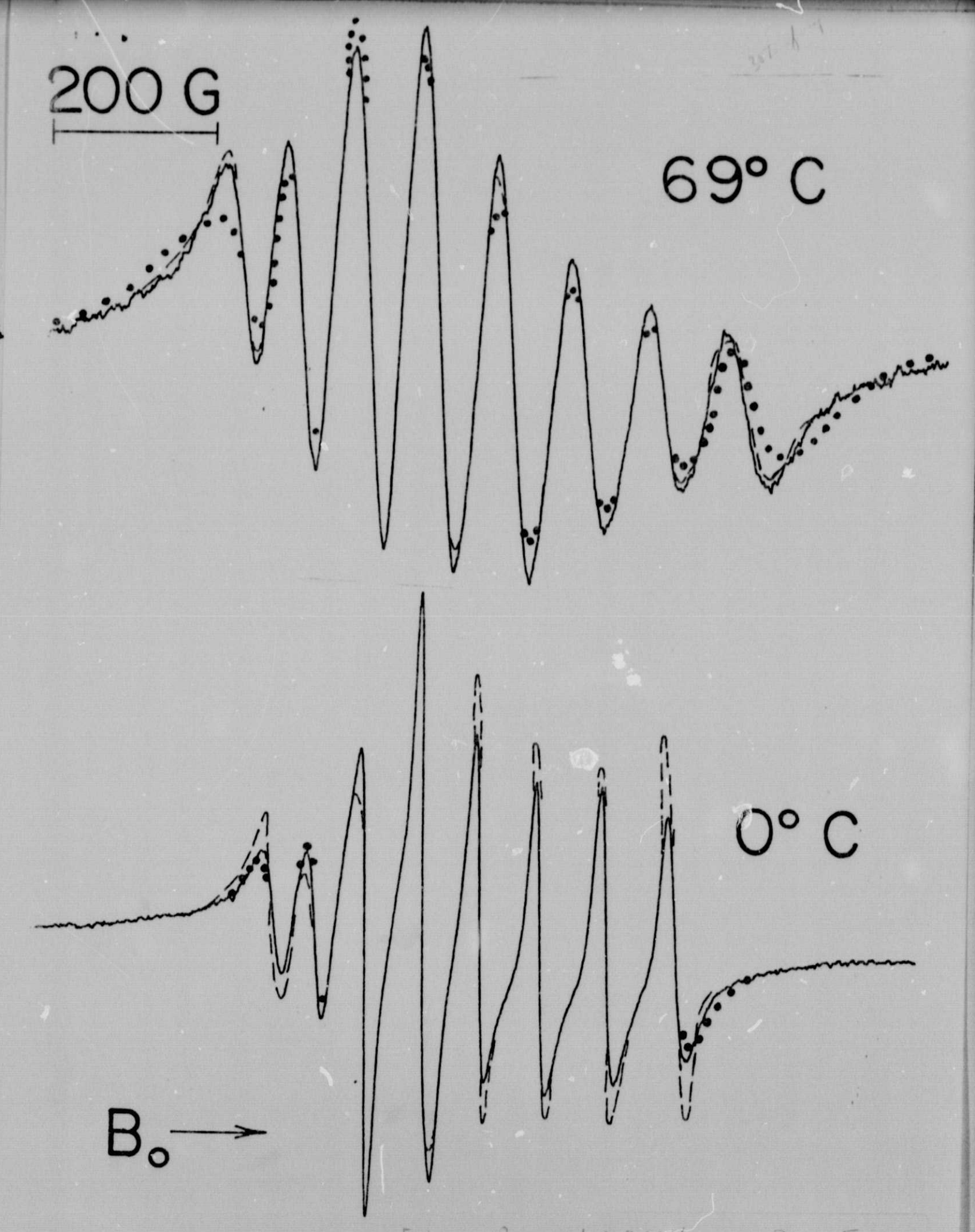

Fig 4 Brandal Sigy PIIMS

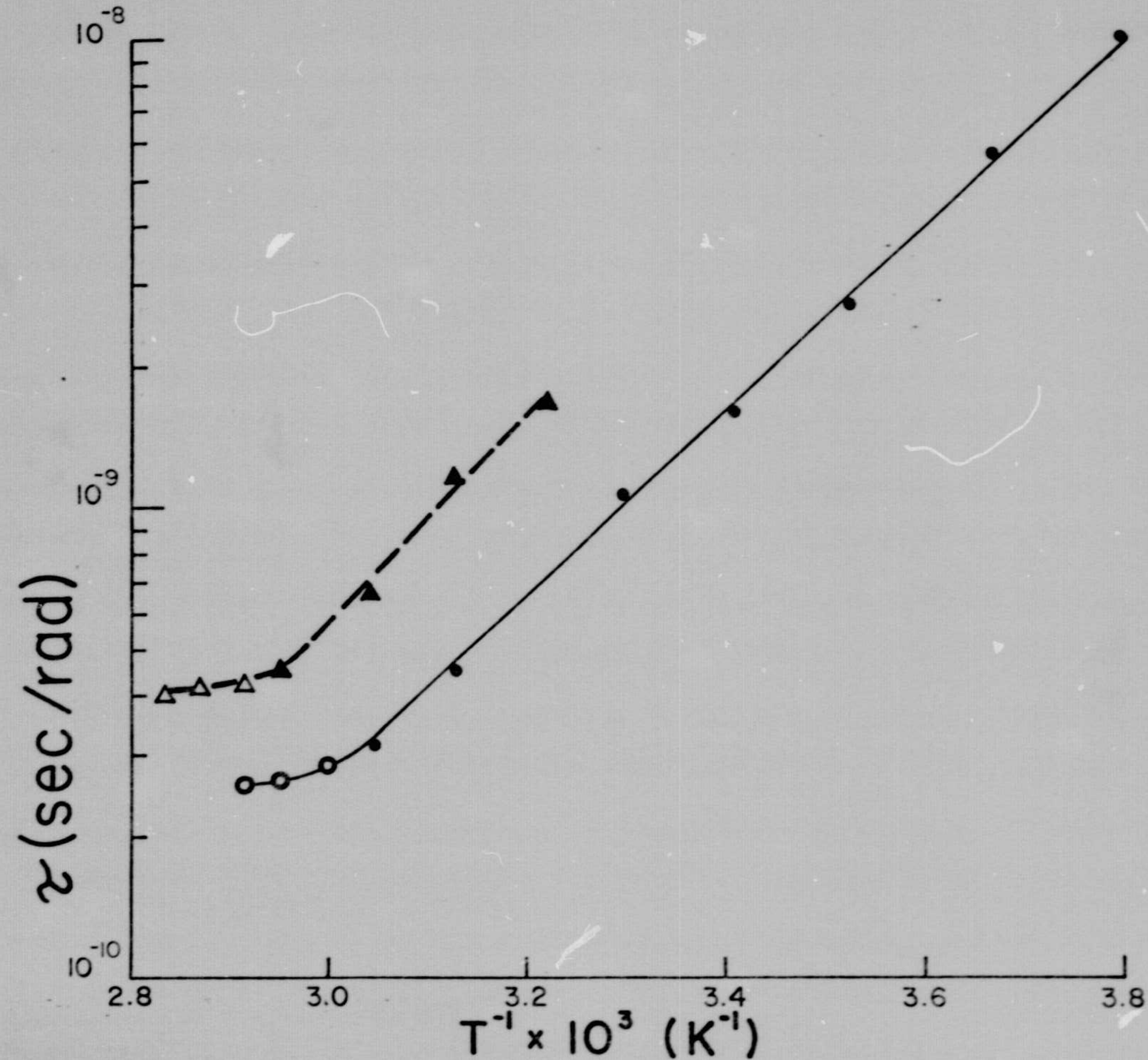

Fig 5 P11M5

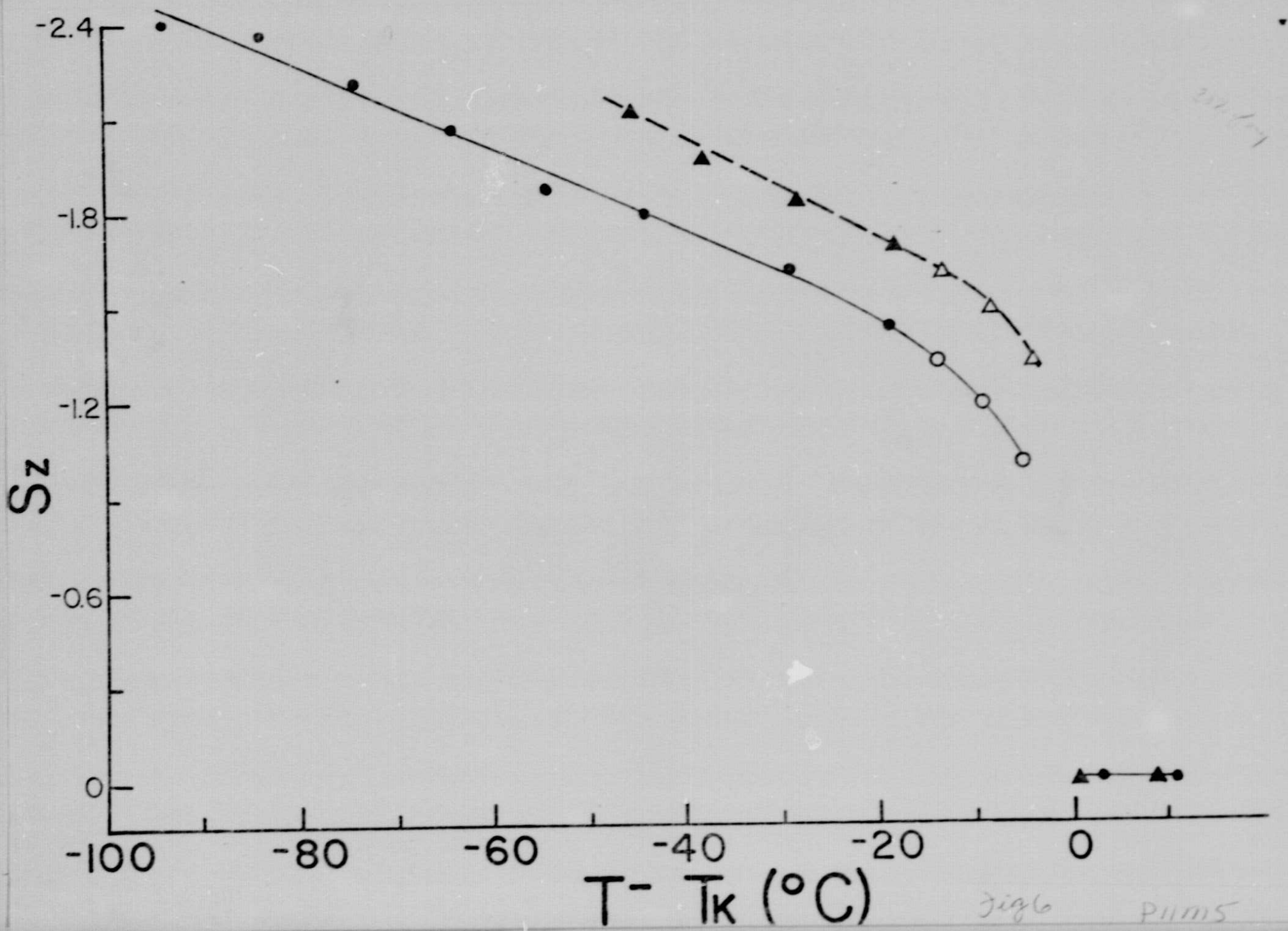

fig 6 PHMS